Journal of Molecular Structure 1155 (2018) 11–20

Contents lists available at ScienceDirect

Journal of Molecular Structure

journal homepage: http://www.elsevier.com/locate/molstruc

New Cu (II), Co(II) and Ni(II) complexes of chalcone derivatives: Synthesis, X-ray crystal structure, electrochemical properties and DFT computational studies

Salima Tabti [a, b, *], Amel Djedouani [c, d], Djouhra Aggoun [e], Ismail Warad [f], Samra Rahmouni [g], Samir Romdhane [h], Hosni Fouzi [i]

[a] Faculty of Science and Technology, Mohamed el Bachir El Ibrahimi University, El Anasser, 34000, Bordj Bou Arreridj, Algeria
[b] Laboratory of Electronic Materials and Systems, Mohamed El Bachir University El Ibrahimi, El Anasser, 34000, Bordj Bou Arreridj, Algeria
[c] Laboratory of Analytical Physicochemistry and Cristallochemistry of Organometallic and Biomolecular Materials, Constantine University 1, 25000, Constantine, Algeria
[d] Superior School of Constantine, University City Ali Mendjeli, 25000, Constantine, Algeria
[e] Laboratory of Electrochemistry, Molecular Engineering and Catalysis Redox (LEIMCR), Department of Engineering Sciences, Faculty of Technology, Farhat University ABBAS de Sétif-1, Algeria
[f] Department of Chemistry, AN-Najah National University, PO Box 7, Nablus, Palestine
[g] Faculty of Sciences, University Farhat ABBAS of Sétif-1-El Bez, Algeria
[h] Laboratory Advanced Materials and Quantum Phenomena, Faculty of Sciences of Tunis, Tunisia
[i] Direction Radiation, Energy and Materials, National Center for Nuclear Science and Technology (CNSTN), Technological Pole, 2020 Sidi Thabet, Tunisia

ARTICLE INFO

Article history:
Received 29 May 2017
Received in revised form
21 October 2017
Accepted 24 October 2017
Available online 27 October 2017

Keywords:
Metal complexes
X-ray crystal structure
Electrochemistry
Quantum chemical calculations (DFT)
Hirschfeld surface

ABSTRACT

The reaction of nickel(II), copper(II) and cobalt(II) with 4-hydroxy-3-[(2*E*)-3-(1*H*-indol-3-yl)prop-2-enoyl]-6-methyl-2*H*-pyran-2-one (HL) leads to a series of new complexes: **$Ni(L)_2(NH_3)$**, **$Cu(L)_2(DMF)_2$** and **$Co(L)_2(H_2O)$**. The crystal structure of the $Cu(L)_2(DMF)_2$ complex have been determined by X-ray diffraction methods. The Cu(II) lying on an inversion centre is coordinated to six oxygen atoms forming an octahedral elongated. Additionally, the electrochemical behavior of the metal complexes were investigated by cyclic voltammetry at a glassy carbon electrode (GC) in CH_3CN solutions, showing the quasi-reversible redox process ascribed to the reduction of the M^{II}/M^{I} couples. The X-ray single crystal structure data of the complex was matched excellently with the optimized monomer structure of the desired compound; Hirschfeld surface analysis supported the packed crystal lattice 3D network intermolecular forces. HOMO/LUMO energy level and the global reactivity descriptors quantum parameters are also calculated. The electrophilic and nucleophilic potions in the complex surface are theoretically evaluated by molecular electrostatic potential and Mulliken atomic charges analysis.

1. Introduction

Dehydroacetic acid 'DHA' and its derivatives are an important class of compounds in organic synthesis, especially as starting materials for the preparation of various heterocyclic systems [1–8]. Chalcones analogue of DHA belong to a class of α, β–unsaturated ketones, they are commonly synthesized via the Claisen Schmidts condensation between ketones and aromatic aldehydes in the presence of a strong base [9–12].

In recent years, a number of β-dicarbonyl compounds in which the carbonyl function(s) bonded to olefinic linkage(s) have gained considerable importance [13–16] mainly because of the fact that such compounds are structurally related to the active chemical constituents of several traditional medicinal plants [17–19]. Therefore, synthesis and characterization of such unsaturated carbonyl systems and their metal complexes have tremendous importance. It is well known that dehydroacetic acid and its derivatives like chalcones have a strong ability to form metal complexes that play a prominent role in modern coordination chemistry. These compounds possessing novel structure features, interesting spectral and magnetic properties have been the subject

* Corresponding author. Faculty of Science and Technology, Mohamed el Bachir El Ibrahimi University, El Anasser, 34000, Bordj Bou Arreridj, Algeria. Tel.: +213 663 495 071.
E-mail address: thabti_sa@yahoo.fr (S. Tabti).

https://doi.org/10.1016/j.molstruc.2017.10.084
0022-2860/

of intensive research due to their importance in biological [3], analytical agriculture [10], antimalarial [20], anti-inflammatory [21], anti-leishmanial [22], and anticancer properties [23]. Some chalcones demonstrated the ability to block voltage-dependent potassium channels [24]. Structurally, they are characterized by the linkage of two aromatic rings joining a three carbon α, β unsaturated carbonyl, or enone moiety [25].

Recently, we are particularly interested to the synthesis of α,β-unsaturated compounds derived from DHA and indol-3-carboxaldehyde [26]. As a continuation of our work, we report herein the synthesis and characterization of new nickel(II), copper(II) and cobalt(II) metal complexes. The structure of copper complex was confirmed by single-crystal X-ray diffraction studies. In addition, Hirschfeld surface analysis, HOMO/LUMO energy and DFT/B3LYP methods were used to predict the structural and spectroscopic parameters of the synthesized compound. Finally, the electrochemical behavior of these compounds was investigated by cyclic voltammetry. The general synthesis of these compounds is given in Scheme 1.

2. Experimental

2.1. Materials and instruments

All solvents and chemicals used throughout this work were purchased from commercial sources and used as received without further purification. The synthesis of these complexes was performed by using several solvents like acetone, methanol, chloroform and ether with the following metal salts: $Cu(NO_3)_2.2.5H_2O$, $CoCl_2 \cdot 6H_2O$ and $Ni(CH_3COO)_2 \cdot 4H_2O$ (Aldrich). The purity of the compounds was checked by TLC on pre-coated SiO_2 gel (HF254, 200 mesh) aluminium plates (E Merk) and visualized in UV chamber Infrared spectra were obtained using potassium bromide (KBr) pellets (4000–400 cm^{-1}) on a Shimadzu FTIR spectrophotometer. Electronic spectra in the 200–800 nm range were recorded using a Shimadzu UV-1700 spectrophotometer with DMF as solvent and quartz cell of 1 cm^3 optical path. Elemental analysis was carried out by Std.meth.0803-CHNS method (*Spectropole elementary analysis service B.511 Faculty of Sciences of saint Jerome-Marseille-France*). Melting points of synthesized product were determined with a Banc Kofler 7779 apparatus. Mass spectroscopy was performed with a mass spectrometer SYNAPT G2 HDMS (Waters) equipped with a source of atmospheric pressure ionization (API) pneumatically assisted. Molar conductivity of all complexes was determined in DMSO (10^{-5} M) at room temperature using Conductivity meter inoLab. Cond 7310.

Cyclic voltammetry experiments were carried out in a Metrohm cell of 5 cm^3 using voltalab 40 (potentiostat/galvanostat) PGZ 301. A glassy carbon (GC) electrode (3 mm in diameter) was used as a working electrode and a platinum wire as an auxiliary electrode. All potentials are quoted with respect to the saturated calomel electrode (SCE). All measurements were recorded at room temperature in acetonitrile solutions containing (0.1 M) Tetra-*n*-butylammonium perchlorate (TBAP) as supporting electrolyte.

2.2. Crystal data collection and processing

The crystal and instrumental parameters used in the unit-cell determination and data collection are summarized in Table 3. Crystals of $Cu(L)_2(DMF)_2$ obtained from low evaporation of DMF solution at room temperature. The monocrystals are Triclinic with P-1 space group.

X-ray single-crystal diffraction data were collected at 293 K on a Diffractometre Bruker- Nonius Kappa CCD, equipped with a graphite monochromator using Mo Ka radiation (k = 0.71073 Å).

The structures were solved by direct methods [27] and refined on F^2 by full matrix least-squares techniques using SHELXL-97 program [28]. All non-H atoms were refined anisotropically.

2.3. Computational details

The computational calculations were performed by Gaussian 09 software [29]. Cif file X-ray structure data was taken as a starting point for the calculations [30]. Hirschfeld surfaces theoretical analysis was carried out using CRYSTAL EXPLORER 3.1 program [31].

2.4. Synthesis of the metal complexes

A series of divalent transition metal complexes of chalcone derivatives (Scheme 1) was synthesized according to the following general procedure:

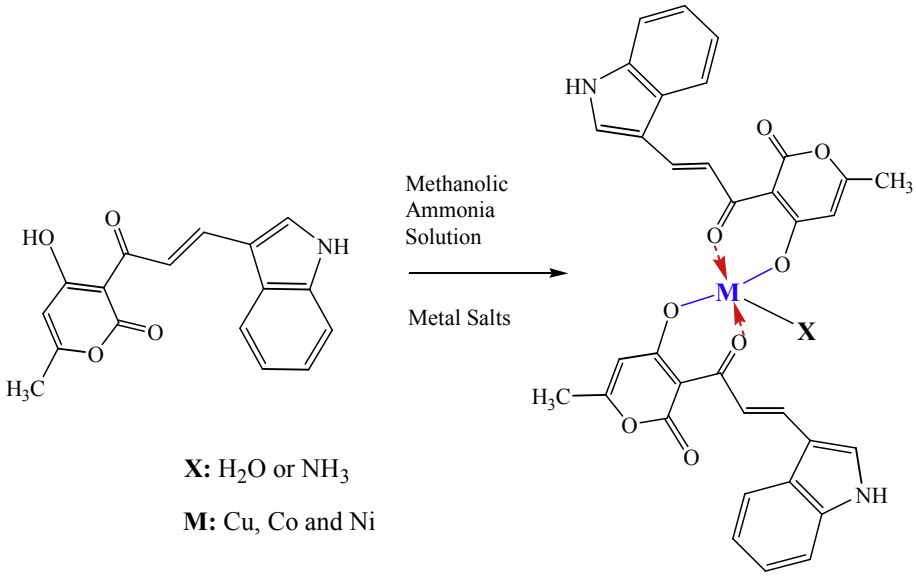

Scheme 1. Reaction way leading to the formation of metal complexes.

➢ **Nickel complex [$C_{34}H_{24}O_8N_2Ni$]** NH_3

Ni $(CH_3COO)_2 \cdot 4H_2O$ (0.062 g, 0.25 mmol, 5 ml, MeOH) was added to the solution of **HL** (0.147 g, 0.5 mmol, 10 ml, $CHCl_3$) under refluxing conditions. The pH of the solution was maintained between 7 and 8 by adding an alcoholic ammonia solution, so 1.5 ml of NH_3 was added to the mixture. The mixture was refluxed for 6 h. The yellow precipitate was filtered and washed successively with ethanol, diethylether.

➢ **Copper complex [$C_{34}H_{24}O_8N_2Cu$]**$\cdot H_2O$

Cu $(NO_3)_2$. $2.5H_2O$ (0.058 g, 0.25 mmol, 5 ml, MeOH) was added to the solution of **HL** (0.147 g, 0.5 mmol, 10 ml, $CHCl_3$). The copper complex appears instantaneously by adding 1 ml of alcoholic ammonia solution. The reflux was maintained for 4 h in order to complete the reaction. The final product was recrystallized from methanol/DMF (80:20) mixtures to obtain single crystals suitable for *X*-ray analysis which were grown at room temperature by slow evaporation of this mixture.

➢ **Cobalt complex [$C_{34}H_{24}O_8N_2Co$]**$\cdot H_2O$

$Co(Cl)_2 \cdot 6H_2O$ (0.059 g, 0.25 mmol, 5 ml to th MeOH) was added e solution of **HL** (0.147 g, 0.5 mmol, 10 ml, $CHCl_3$). The pH of the solution was maintained between 7 and 8 by adding alcoholic ammonia solution, so 2 ml of NH_3 was added to the mixture. It was refluxed for 1 h, the gold complex was obtained with the above described procedure.

3. Results and discussion

3.1. Chemistry

Analytical data indicated that the condensation of dehydroacetic acid and indole-3-carboxaldehyde occurred in 1:1 ratio to form the 4-hydroxy-3-[(2*E*)-3-(1*H*-indol-3-yl)prop-2-enoyl]-6-methyl-2*H*-pyran-2-one [32]. All the complexes were obtained as solids in different yields. They are analytically pure, stable in air at room temperature and possess good keeping qualities. They are insoluble in acetone, ethanol and chloroform, but their considerable solubility has been noticed in acetonitrile, DMF and DMSO. The elemental analyses are in good agreement with the expected stoichiometry of complexes, which indicate that the metal with ligand ratio in all complexes is 1:2 (Table 1)

3.2. Spectral characterization

The characteristic FT-IR frequencies (cm^{-1}) of the ligand and their complexes are shown in Table 2. The ligand has a strong band at 3210 cm^{-1} corresponding to the νOH (phenolic hydrogen bond) stretching frequency. The band observed around 1680 cm^{-1} is assigned to ν C=O (lactone carbonyl) of **HL**. This strong band is shifted to a higher wave in the spectra of metal (II) complexes. This indicates the coordination of keto (C=O) and hydroxyl groups to the metal atom in complexes. In the spectra of the complexes, the appearance of new bands in the region 600–450 cm^{-1} can be attributed to ν M – O bands [33,34].

The UV–Vis absorption spectra show the modification of the absorption bands characteristic of the ligand (Fig. 1), as well as the occurrence of some new bands, characteristic for the formation of the coordinative compounds. The UV–Vis band observed for **HL** exhibits electronic transitions with strong band at 285 nm, was assigned to $\pi-\pi^*$ aromatic group transitions [10,32,35] which remains almost unchanged in the complexes. The low intensity band observed at 332 nm is due to (–CH=CH) chalcone group and the transition at 345 nm is assigned to $n-\pi^*$ carbonyl group transition. The last intense band at 438 nm is probably assigned to $n-\sigma^*$ hydroxyl group of ligand transitions. In the copper and nickel complexes, these bands experience a bathochromic shift, as for the cobalt complex, it shifts to hypsochromic. This displacement is due to the coordination of carbonyl group with metal ions. In Co(II), Ni(II) and Cu(II) complexes a shoulder is observed between 350 and 430 nm that can be assigned to ligand to metal charge transfer transitions (LMCT) [36].

The molar conductivity of all synthesized complexes was showed in (Table 1). The low conductance of the chelate solution in DMSO supports the non-electrolyte nature of the metal complexes and there is no counter ion present outside the coordination sphere of complexes [10,13,37].

ESR spectroscopy has proven to be a powerful technique revealing three important types of information about the environment of the complexes, the nature of the ligand types, the distortion of the complexes and degree of association within

Table 1
Elemental analysis and some physical data of metallic complexes of **HL**.

Compound	Color	Yield %	Elemental analysis (calcd) %				M.P °C	γ μs/cm²mol⁻¹	Mass spectra
			C	H	N	O			
$C_{17}H_{13}O_4N$	Orange	60	65.04 (65.17)	4.05 (4.79)	4.42 (4.47)	21.69	224.7	–	294.87
[$C_{34}H_{24}O_8N_2Cu$]. H_2O	Red brick	70	61.31 (60.94)	4 .9 (3.91)	3.75 (4.18)	21.89	260	2.8	652.0898
[$C_{34}H_{24}O_8N_2Ni$]. NH_3	Yellow	75	60.62 (61.47)	5.33 (4.10)	6.81 (6.33)	17.66	305	2.2	647.0957
[$C_{34}H_{24}O_8N_2Co$]. H_2O	Gold	65	61.10 (61.36)	3.73 (3.94)	4.68 (4.21)	19.92	267	2.6	648.0938

Table 2
Infrared absorptions bands of the ligand (**HL**) and its metal complexes.

	ν NH	ν OH	ν C=O (lactone)	ν C=O–C=C acetyl carbonyl	ν C–N ind	ν C–*O*–C	ν C=O coord.	ν M-O
HL	3080	3210	1684	1648	1650,1530	1088	–	–
[$C_{34}H_{24}O_8N_2Cu$]	2998	3430	1700	1680	1535	1043	1272	670
[$C_{34}H_{24}O_8N_2Ni$]	3000	3400	1678	1653	1550	1150	1270	782
[$C_{34}H_{24}O_8N_2Co$]	2950	3416	1690	1650	1550	1189	1270	764

Table 3
Crystallographic data and structure refinement details for compound **Cu (L)$_2$(DMF)$_2$**.

Name	**Cu(L)$_2$(DMF)$_2$**
Formula	$C_{40}H_{38}$ CuN_4O_{10}
Formula weight	798.28
Space group	*P*-1
F(000)	512
Crystal system	Triclinic
Unit cell dimensions	
a (Å)	8.996(5)
b (Å)	9.817(5)
c(A°)	11.843(15)
α; deg	73.219(5)
β; deg	72.298(5)
γ; deg	85.547(5)
V; Å^3	953.888(8)
Z	2
Temperature(K)	293 (2)
θ Range for data collection (°)	5.6–73.6°
Crystal size (mm)	0.1 × 0.1 × 2
Wavelength ((Mo *Kα*)(Åmm-1)	1.240
D_{calc} (g cm^{-3})	1.59
μ(mm^{-1})	0.901
hkl range	$-13 \le h \le 13$
	$-14 \le k \le 14$
	$-17 \le 1 \le 18$
Ref Nmb of reflections measured	20580
Number of independent reflections (*R*int)	2279
Number of parameters	161
reflections with $I > 2\sigma(I)$	20580
Refinement method	Full-matrix least-squares on *F*2
Goodness-of-fit (GOF) on *F2* (S)	1.068
R [*F2* > 2 *σ* (*F2*)]	0.077
w*R(F2)*	0.2039
R_{int}	0.041
Absorption coeff. (mm^{-1})	0.81
Max/min δ*p* (e/Å^3)	0.16/-0.18

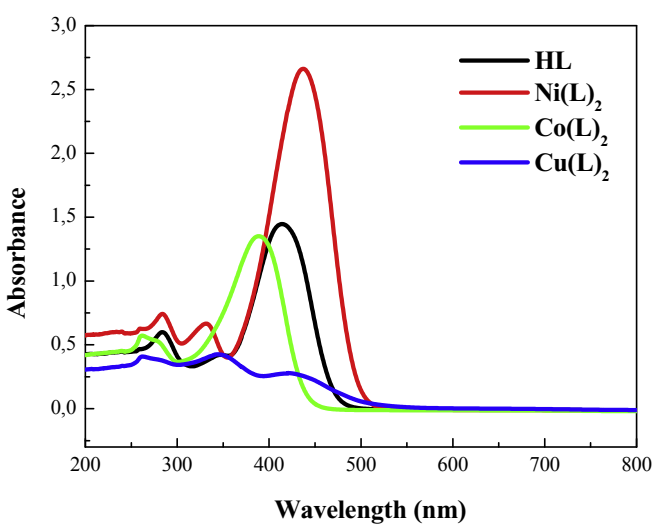

Fig. 1. UV–Vis spectra of **HL** and its metal complexes.

system [38]. The ESR spectrum of the representative Cu^{II} complex is recorded at room temperature and in DMSO (Fig. 2). The analysis of the spectrum gives $g_0 = 2.0628$, $g_\perp = 2.3317$ and $g_{II} = 2.4762$ and the value of ΔH_{PP} (G) = 14.1940 10^5. The trend $g_{II} > g_\perp > g_e$ observed for the complex indicates the octahedral geometry that from the data, the considerable covalent character of metal–ligand in the complex is predicated, and from the observed 'g' values it is evident that the unpaired electron lies predominantly in the d_{x2-y2} orbital [39] with a possibility of some dz^2 character being mixed with it because of

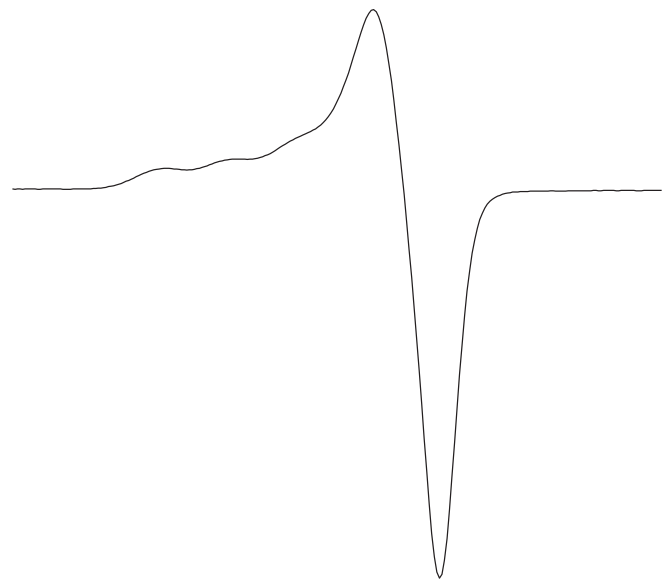

Fig. 2. The ESR spectrum of copper complex at room temperature.

low symmetry [40].

3.3. X-ray crystallographic study

The perspective representation of the complex Cu(L)$_2$(DMF)$_2$ with the atom numbering is given in (Fig. 3a).

The complex **Cu (L) $_2$(DMF)$_2$** crystallized in a triclinic system in P-1 space group with two units per cell (Z = 2) **(**Fig. 3 A**)**. The Centro symmetric structure consists of the neutral complex species **Cu(L)$_2$(DMF)$_2$**. The Cu(II) lying on an inversion center is coordinated to six oxygen atoms forming an octahedral elongated [41]. The bidentate (HL) ligand deprotonated occupies the equatorial plane of the complex in a trans configuration, each chelating the metal through four atoms, 2O (1), and 2O (2) form the equatorial plane of

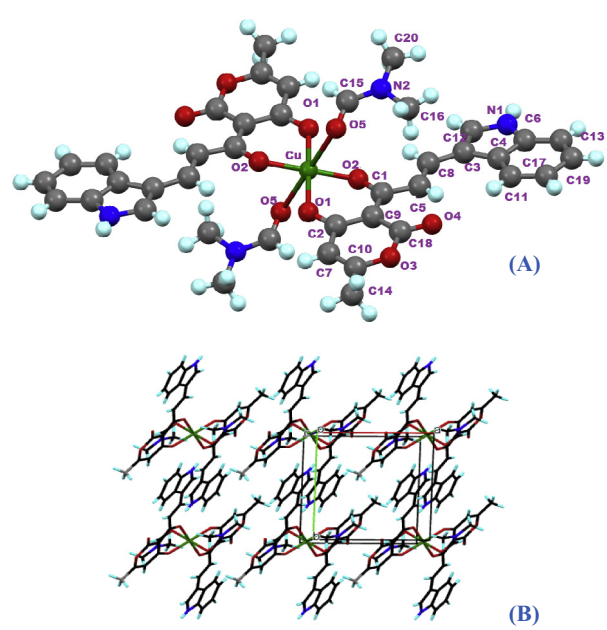

Fig. 3. Crystal structure and atoms numbering for **Cu (L)$_2$(DMF)$_2$ (A)**; Packing of molecules along the (c) direction **(B)**.

the octahedron and two other atoms 2O (5) (dimethylformamide molecules) are in axial position. The distances of the bonds Cu–O (1) = 1.911(16) Å, Cu–O(2) = 1.910 (16) Å, and Cu–O (3) = 2.635(17) Å are consistent with the distance of these bonds in the copper(II) complexes described by Hong Liang [42] and Wen-Xing Zhang [43]. In the network (Fig. 3b), the complex molecules are lying in layers made of parallel planes. Dimethylformamid molecules occupy the free space between the planes. The stacking and the cohesion of the crystal are provided by the presence of intermolecular hydrogen bonds via the dimethylformamide molecules.

3.4. Electrochemical behavior

Cyclic voltammetry is the most widely used technique to investigate qualitative information about electrochemical reactions. The electrochemical properties of the synthesized compounds were studied by cyclic voltammetry in 10^{-1} M of TBAP and 10^{-3} M of each synthesized compound using a glassy carbon electrode. The voltammogram of the ligand **HL** recorded in the potential range from −1.6 V and +1.6 V vs. SCE shows two oxidation waves. The first is located at 0.46 V vs. SCE probably attributed to the oxidation of the chalcones [44] group while the second wave (at 1.31 V vs. SCE), is ascribed to the oxidation of the hydroxyl function. Thus, at more negative potential, a reduction wave with peak potential of −1.28 V vs. SCE, was observed that could be attributed to the reduction of chalcones [45] (Fig. 4 A).

The cyclic voltammograms of the synthesized metal complexes were also recorded in acetonitrile solution within the potential range from −1.6–1.6 V vs. SCE at a scan rate of 100 mV/s. The voltammogram of copper complex **Cu (L)$_2$** shows three oxidation waves, observed at $Ep_{a1} = -0.70$, $Ep_{a2} = 0.31$ and $Ep_{a3} = 1.03$ V vs. SCE, respectively. The first wave is due to reoxidation of the Cu(I) to Cu(II). The second irreversible oxidation wave is attributed probably to the oxidation of the Cu(II) to Cu(III). As for the last oxidation wave, it was probably referred to the oxidation of the ligand. There is only one reduction peak located at −1.00 V vs. SCE due to reduction of Cu(II) to Cu(I) [46]. As for the nickel complex, two oxidation waves have been observed and located respectively at $Ep_{a1} = -0.70$ and $Ep_{a2} = 1.28$ V vs. SCE, respectively. The first wave is due to re-oxidation of the species Ni(I) to Ni(II) and the second wave is due to the oxidation of the ligand. One cathodic peak at $Ep_c = -1.03$ V vs. SCE, which is due to the reduction of Ni(II) to Ni(I). The cyclic voltammogram of cobalt complex shows a similar remarkable behavior except a slight shift of peak potentials with an

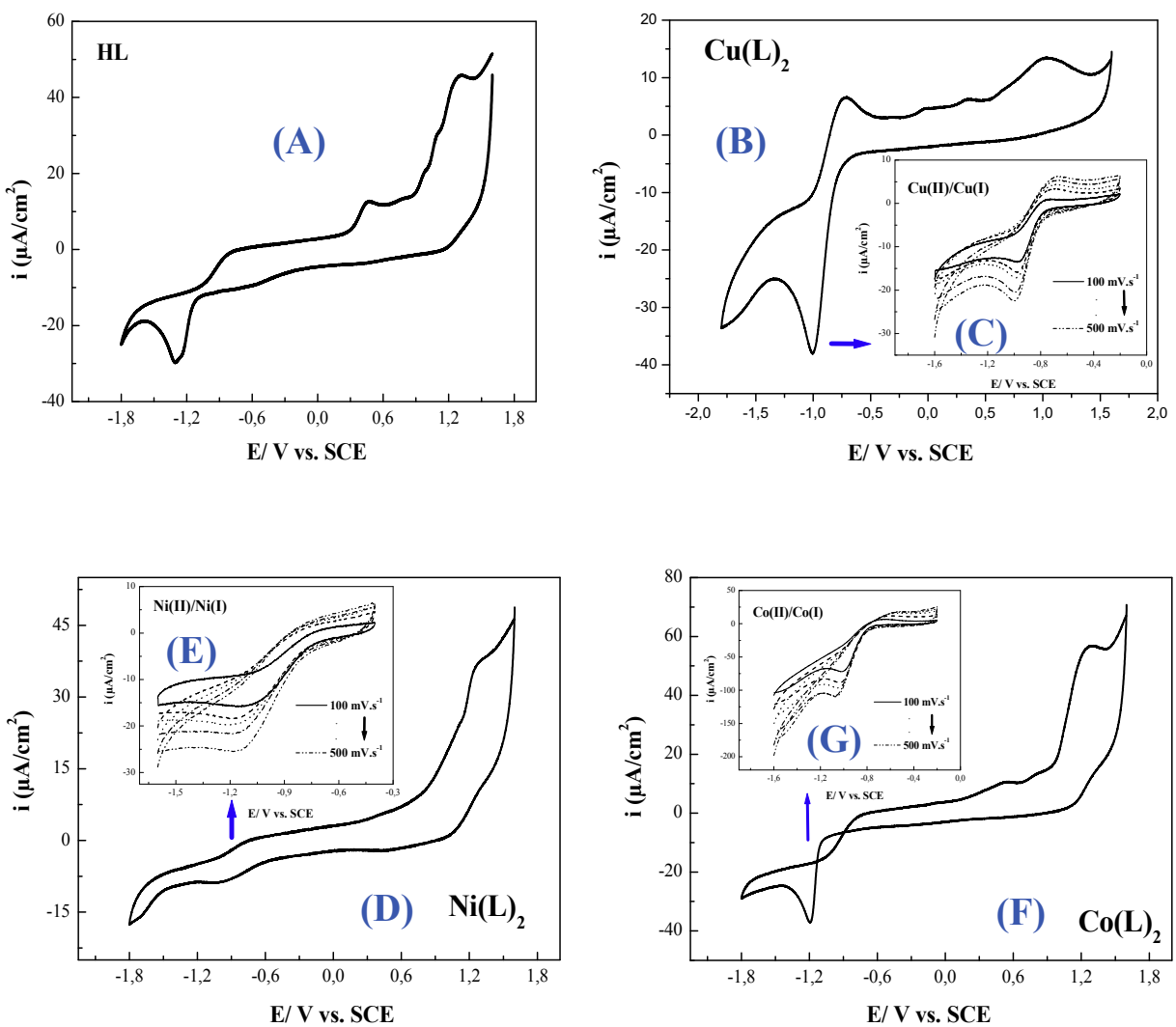

Fig. 4. Cyclic voltammogram of **HL** at a glassy carbon electrode in acetonitrile medium (10^{-3} mol/L) (10^{-1} mol/L TBAP) (**A**); Cyclic voltammograms of the copper (**B**), nickel (**D**) and cobalt (**F**) complexes in same experimental conditions. Cyclic voltammograms of M(II)/M(I) redox couple showing the effect of the scan rates: of the copper (**C**), nickel (**E**) and cobalt (**G**) complexes.

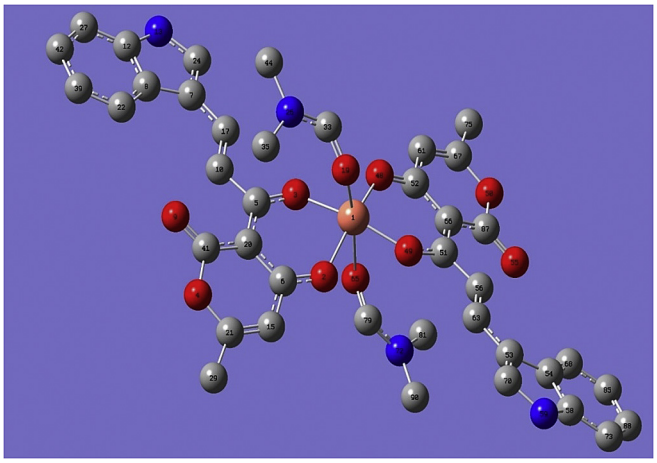

Fig. 5. Structure of the title compound, optimized ground state geometry at B3LYP/3-31G level of theory.

irreversible oxidation wave located at $Ep_a = 1.26$ V vs. SCE attributed to the oxidation of the ligand and also one reduction peak at $Ep_c = -1.18$ V vs. SCE attributed to the reduction of Co(II) to Co(I) [47].

For the copper complex, we have followed the evolution of potentials of anodic and cathodic peak currents depending on the variation of the scan rates for the Cu(II)/Cu(I) redox system by cycling between − 0.2 and - 1.6 V vs. SCE. In this case, an obvious increase of intensities of the (ip_a, ip_c) peak currents was observed as the scan rate increase. The peak to peak separation seems to be greater than 60 mV. Therefore, this suggested that this redox system is not Nernstian. In addition, it was found that the peak currents obtained present a linear dependence versus the square root of the scan rate as it is expected for a controlled diffusion reaction. The cathodic reductions waves presented in both other complexes (nickel and cobalt) were also achieved by cycling between −0.2 and −1.6 V vs. SCE of the potential at the vitreous carbon electrode surface at different scan rates. The resulting M(II)/M(I) redox system seems to have an irreversible redox couple for these complexes (Fig. 4).

3.5. DFT calculation

3.5.1. X-ray crystal and optimized structure

The molecular structure of the desired complex was optimized as monomer compound with B3LYP/3-31G(d), as can be seen in (Fig. 5). Neutral octhedral geometrical structure around the copper(II) center was opserved, six oxygen atomes corrdenated the copper center. The DMF solvent molecules coordentated the center through the O atoms and no N atoms in trans mode with O−Cu−O 175° angle. The crystal experimental data and selected geometric parameters (bond lengths and angels (°)) of the desired complex are listed in (Table 4).

The structure of the title complex was solved by X-ray single crystal analysis, there is a good chance to compare the XRD structure parameters like bond lengths and their angles with the DFT/B3LYP/optimized structure as can be seen in Fig. 6. In addition, good matching between theoretical and experimental result was collected (Fig. 6). This figure shows the relation between the XRD experimental and DFT calculated bond lengths. The XRD data revealed Cu−O(DMF) with longer distances compared to the DFT, the other bonds showed excellent matching. Moreover, the experimental angles are totally matched with the DFT calculated data.

3.5.2. Hirshfeld surface analysis for the complex

Using the cif file crystal structure information of the desired complex Hirshfeld surface theoretical calculation was carried out, the sufficient intermolecular forces and $atoms_{inside}/atom_{outside}$ fingerprint map interactions were illustrated in Figs. 7 and 8 respectively. Fig. 7 showed surfaces mapped over a d_{norm}, d_e and d_i [48,49]. The red dark-spots on the d_{norm} surface revealed the shortness and strongest one type of H-bond interactions, C−H … O with distance = 2.619, 2.662, 2.722 Å as polar H-bonds and several non-polar interaction such C−H …. H/C van-der-Waals interactions [48−50]. The Hirshfeld surface result is consisted with the X-ray packing mode in the crystal lattice.

The 2D-fingerprint plots over the Hirshfeld surfaces of the complex revealed the most important differences between the interaction patterns. Total interactions, H … all atoms pediment with 64.3%, classified as H … H (47.3%), H … C (8.3%), H … O (8.1%), H … N (0.3%) and H … Cu (0.0%), were illustrated in Fig. 8.

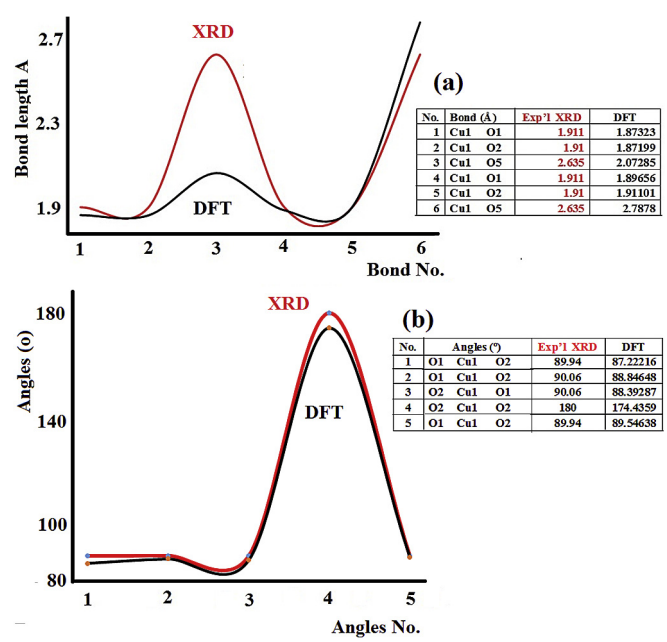

Fig. 6. Graphical relation between XRD experimental versus the DFT calculated bond lengths and angles (a, b) respectively.

Table 4
The XRD experimental bond lengths (**Å**) and angels (°) together with the calculated B3LYP/3-31G.

Bond (Å)	Exp'l XRD	DFT/B3LYP 3-31	Angle (°)	Exp'l XRD	Angle (°)	DFT/B3LYP 3-31G
Cu1−O2	1.9101	1.9110	O2−Cu1−O2	180.00(6)	O1−Cu1−O2	87.22216
Cu1−O2	1.9101	2.7878	O2−Cu1−O1	90.07(7)	O1−Cu1−O2	88.84648
Cu1−O1	1.9107	1.8966	O2−Cu1−O1	89.93(7)	O2−Cu1−O1	88.39287
Cu1−O1	1.9107	1.8721	O2−Cu1−O1	89.93(7)	O2−Cu1−O2	174.4359
Cu1−O5	2.6350	1.8732	O2−Cu1−O1	90.07(7)	O1−Cu1−O2	89.54638
Cu1−O5	2.6350	2.0728	O1−Cu1−O1	180.0(1)		

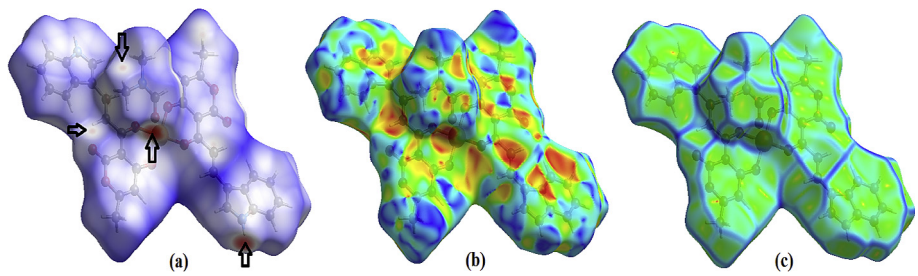

Fig. 7. (**a**) d_{norm}, (**b**) shape index and (**c**) curvedness on Hirshfeld surface intermolecular forces belongs to the complex.

3.5.3. Molecular electrostatic potential MEP investigation

MEP map is very helpful graph to present the nucleophilic and electrophilic positions and figure out the preferred positions for the Hydrogen bonding interactions (Fig. 9). The blue and red indicating the H-acceptor and donor sites interactions, respectivily. The blue regions indicated the electrophile (electron poor) regions, while the red is nucleophile (electron rich). In the structure of the desired compound the six oxygen atoms revealled the most nuclophilic site due to the free electrons lone pair (that is consisted with HAS result). The free lone pair electrons of pyrol nitrogen atom refelected electrophilic site (blue) which means it is free enough and mostly in engaged in ring delocalization. Protons of methyl and phenyls groups gave green color with electrophilic moderite.

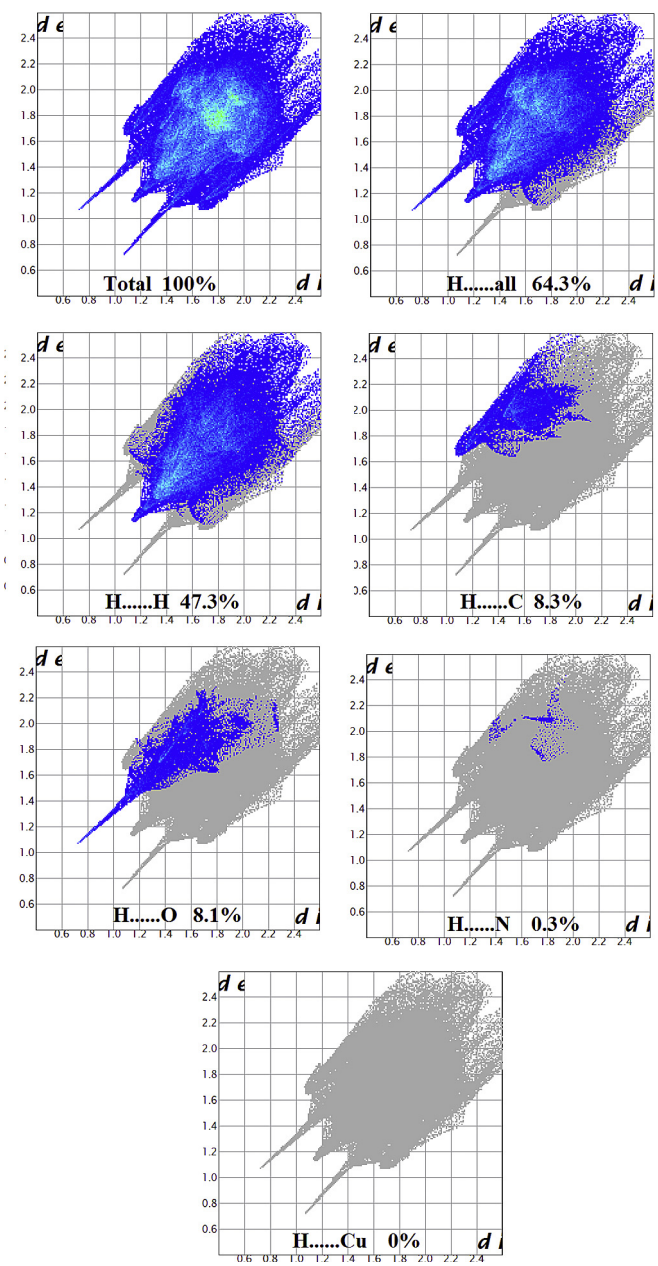

Fig. 8. Hirshfeld surface fingerprint atom … atom.

3.5.4. Mulliken atomic charge population analysis

The atomic charge distribution of acceptor and donor atoms in molecules effected directly many quantum theoretical parameterizes like: polarizability, refractivity dipole moment, and electronic structural parameters [50]. Mulliken population charge analysis of the desired compound was performed by B3LYP, as shown in Table 5 and Fig. 10. The analysis revealed the presence of +ve, acceptor (electrophilic) and -ve, donor (nucleophilic) atomic charge. The electrophilic charge are localized at all the hydrogen atoms ~ (+0.10–0.23e) and the six carbonyl carbon atoms revealed an electrophilic behavior ~ (+0.40–0.60) values, The carbon atoms in the complex mostly revealed nucleophilic behavior due to the electrons delocalization in the aromatic and unsaturated bonds in the backbone of the organic ligand, the phenyl and pyrrole electrons delocalized effected the nuclophilicity of all the ring carbon atoms (−0.10–0.30 e). The analysis revealed the high electronegative O atoms with high nuclophilicity amounts −0.40–0.6 e, meanwhile the N atoms of pyrrole are with the highest nuclophilicity −0.81e. This result is highly consisted with the HAS analysis and MPE map.

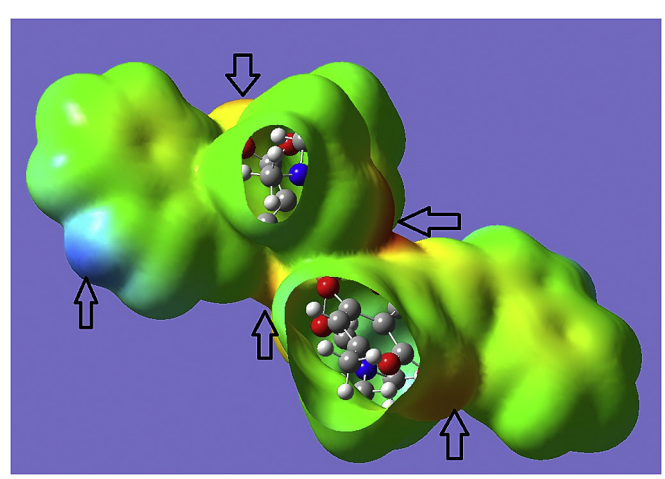

Fig. 9. The molecular electrostatic potential (MEP) graph.

Table 5
Mulliken atomic charges.

No.	Atom	DFT/B3LYP/3-31G(d)	No.	Atom	DFT/B3LYP/3-31G(d)	No.	Atom	DFT/B3LYP/3-31G(d)
1	Cu	0.704714	32	H	0.208009	63	C	−0.185869
2	O	−0.621833	33	C	0.503865	64	H	0.225999
3	O	−0.600941	34	H	0.205324	65	O	−0.472053
4	O	−0.555698	35	C	−0.415804	66	C	−0.217821
5	C	0.447805	36	H	0.204273	67	C	0.349668
6	C	0.482693	37	H	0.252798	68	C	−0.259730
7	C	−0.049124	38	H	0.242838	69	H	0.235055
8	C	−0.010836	39	C	−0.183611	70	C	0.105349
9	O	−0.515612	40	H	0.189308	71	H	0.219697
10	C	−0.286492	41	C	0.649304	72	N	−0.612682
11	H	0.253656	42	C	−0.189376	73	C	−0.189225
12	C	0.361136	43	H	0.185137	74	H	0.175868
13	N	−0.810731	44	C	−0.381189	75	C	−0.598450
14	H	0.325825	45	H	0.210924	76	H	0.228978
15	C	−0.270904	46	H	0.242845	77	H	0.230249
16	H	0.202959	47	H	0.210838	78	H	0.206034
17	C	−0.186650	48	O	−0.632566	79	C	0.463634
18	H	0.230250	49	O	−0.624816	80	H	0.195648
19	O	−0.512977	50	O	−0.558412	81	C	−0.406113
20	C	−0.227141	51	C	0.453948	82	H	0.189534
21	C	0.348408	52	C	0.508706	83	H	0.232993
22	C	−0.259183	53	C	−0.046258	84	H	0.225969
23	H	0.231065	54	C	−0.012125	85	C	−0.183846
24	C	0.107266	55	O	−0.516007	86	H	0.188762
25	H	0.222009	56	C	−0.289347	87	C	0.657523
26	N	−0.604255	57	H	0.261736	88	C	−0.189511
27	C	−0.188783	58	C	0.361216	89	H	0.183703
28	H	0.177564	59	N	−0.811215	90	C	−0.370611
29	C	−0.598843	60	H	0.324444	91	H	0.195919
30	H	0.232601	61	C	−0.267915	92	H	0.226691
31	H	0.229910	62	H	0.201727	93	H	0.202185

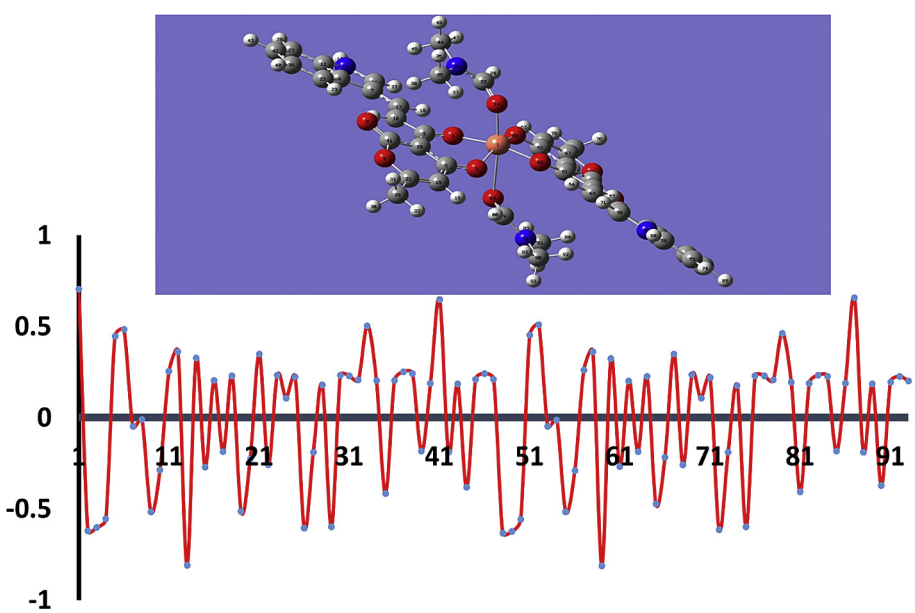

Fig. 10. Mullikan charges distribution of each atoms in the desired compound B3LYP/3-31G(d) values.

3.5.5. HOMO-LUMO

The FMOs manipulate a serious turn in the electric and optical properties, quantum calculation and UV–Vis electron transfer behavior [51]. Small FMOs gap molecules generally less kinetic stability but more polarized and reactivated compounds [52,53]. The ionization potential of molecule concerning directly with HOMO energy, which pointed out the electron donating capacity. Meanwhile, the electron affinity related to LUMO energy degree of electrons acceptation. With the assistance of DFT theoretical calculation HOMO and LUMO shapes and energies levels for the compound were evaluated, as shown in (Fig. 11). Global reactivity descriptors (GRD) can be easily calculated from the energy gaps levels, which facilitated analysis and understanding the structural activities of the desired molecule.

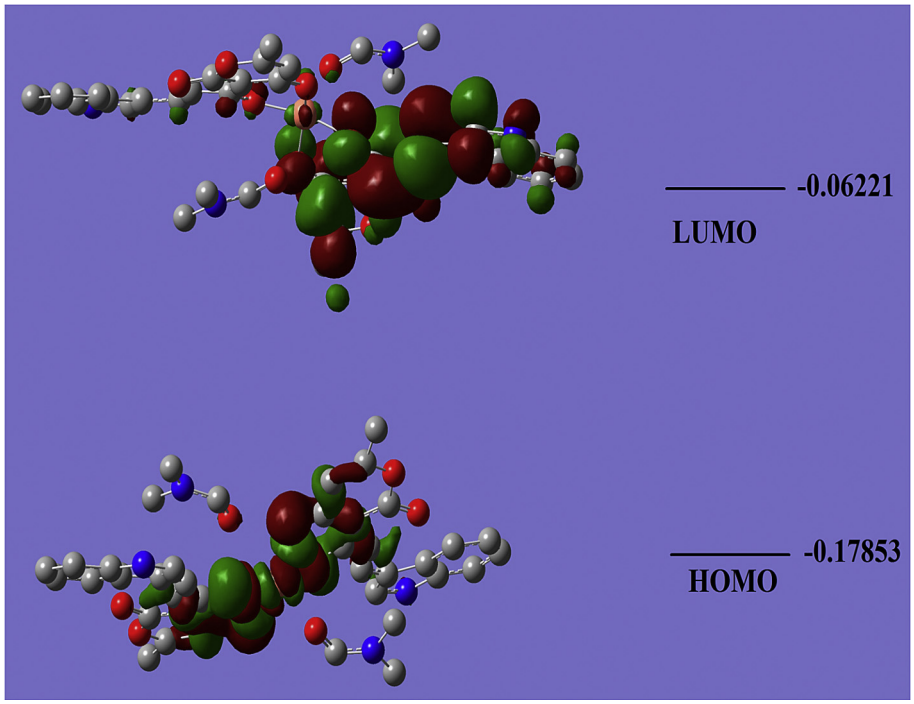

Fig. 11. HOMO→LUMO shape and energy level diagrams (a) DFT/B3LYP/6-31G(d) and (b) HF/6-31G(d).

Table 6
DFT/B3LYP calculated GRD quantum parameters.

	DFT/B3LYP/6-31G(d)
E(a.u.)	−4137.37856671
E_{HOMO}(eV)	−4.858051
E_{LUMO}(eV)	−1.692821
ΔE(eV)	3.165230
X(eV)	3.27654
η(eV)	3.22073
σ(eV)	0.31056
μ(eV)	−3.27652
ω(eV)	1.66654
D(Debye)	3.26472

3.5.6. GRD quantum parameters

The GRD of the desired molecule like electrophilicity (*ω*), hardness (*η*) electronegativity (χ), chemical potential (μ) and softness (σ) indexes, as helpful quantum parameters were calculated from HOMO/LUMO energy gap at both of DFT and HF level of theory (Table 6) using Koopman's notation as follow:

Electronegativity (χ) = - E_{HOMO} + - E_{LUMO}/2

Hardness (η) = ELUMO + - E_{HOMO}/2

Softness (σ) = 1/η

Chemical potential (μ) = - χ

Electrophilicity (ω) = μ2/2η

The value of chemical potential revealed the stability and non-spontaneous decomposition of the molecule. The hardness value of the molecule contemplated the polarizability with sufficient amount that make it a soft compound with faster electrons transfer, the electronic attraction power was indicated by electrophilicity and electronegativity values.

4. Conclusion

In summary, we have successfully synthesized and characterized new series of metallic complexes derivatives of α, β-unsaturated ligand, the production of a this compound may be achieved by a condensation reaction of DHA with Indol-3-carboxaldehyde. The ligand behaves as bidentate, coordinating through the phenolic oxygen and the acetyl carbonyl group of the dehydroacetic acid moiety. The characterization of all compounds was found by physicochemical and spectroscopic methods as elemental analysis, FT-IR, UV–Vis and Masse spectrum. The electrochemical behavior of the metallic complex was investigated with cyclic voltametry using glassy carbon (GC) as working electrode in acetonitrile solution. The crystal structure of the copper complex has been determined by single x-ray diffraction, this complex crystallizes in triclinic space group P-1. HOMO/LUMO energy level and the global reactivity descriptors quantum parameters are also calculated.

Acknowledgments

The Authors gratefully acknowledge the financial support from The Algerian Ministry of Higher Education and Scientific Research, and to Dr. Jean-Luc Parrain, Dr. Michel Giorgi, Dr Valerie Monnier and Christophe Chendo, from Aix-Marseille University Campus Saint-Jerome, France for analyses.

References

[1] M. Cindric, T. Kajfez Novak, K. Uzarevic, Molecular and crystal structures of N, N0-propyleneand N,N0-phenylene-diylbis [3-(1-aminoethyl)-6-methyl-2H-pyran-2,4(3H)-dione, J. Mol. Struct. 750 (2005) 135–141.
[2] A. Djedouani, A. Bendaas, S. Boufas, M. Allain, G. Bouet, M. Khan, Zwitterionic (E)-6-methyl-2-oxo-3-[1-(p-tolyliminio)ethyl]-2H-pyran-4-olate, Acta Cryst. E63 (2007) 1271–1273.
[3] M. Cindric, V. Vrdoljak, T.K. Novak, M. Curic, A. Brbot-Saranovic, B. Kamenar, Synthesis and characterization of two dehydroacetic acid derivatives and molybdenum(V) complexes: an NMR and crystallographic study, J. Mol. Struct. 701 (2004) 111–118.
[4] M. Sato, T. Oda, K. Iwamoto, S. Fujii, A new method for synthesis of crown

ether type pyridinophanes, Heterocycles 60 (2003) 899–908.
[5] A.E. Kihel, M. Benchidmi, E. Essassi, P. Bauchat, R. Danion-Bougot, Reactivity of amino benzimidazoles with 4-hydroxy-6-methylpyran-2-one and 4-hydroxycoumarine, Synth. Commun. 29 (1999) 2435.
[6] D. Kumar, S.P. Singh, A. Martinez, A. Fruchier, J. Elguero, M. Martinezripoll, J.S. Carrio, A. Virgili, The structure of the compounds resulting from the reaction of arylhydrazines with dehydroacetic acid, an NMR and crystallographic study, Tetrahedron 51 (1995) 4891–4906.
[7] L. Somogyi, Reactions under acylating conditions and formation of fused isoxazole derivatives with concomitant N=N bond cleavage, Liebigs Ann. (1995) 721–724.
[8] G.S.R. Reddy, N.R. Rao Synthesis and thermal studies of mixed ligand complexes of Cu(II), Co(II), Ni(II) and Cd(II) with mercaptotriazoles and dehydroacetic acid, Indian J. Chem. B 33 (1994) 113.
[9] S. Thabti, A. Djedouani, A. Bendaas, S. Boufas, R. Louis, D. Mandon, 4-Hydroxy-6-methyl-3-[3-(thiophen-2-yl)acryloyl]-2H-pyran-2-one, Acta Cryst. E69 (2013) 524–525.
[10] B.T. Thaker, R.S. Barvalia, Bidentate coordinating behaviour of chalcone based ligands towards oxocations: VO(IV) and Mo(V), Spectrochim. Acta A 112 (2013) 101–109.
[11] A.M. Asiri, S.A. Khan, Synthesis, characterization and optical properties of mono- and bis-chalcone, Mater. Lett. 65 (2011) 1749–1752.
[12] A. Solhy, R. Tahir, S. Sebti, R. Skouta, M. Bousmina, M. Zahouily, M. Larzek, Efficient synthesis of chalcone derivatives catalyzed by re-usable hydroxyapatite, Appl. Catal. A- Gen. 374 (2010) 189–193.
[13] (a) V.N. Patange, B.R. Arbad, Synthesis physico-chemical and antimicrobial screening studies of some transition metal complexes with O: O donor ligand, Transit. Met. Chem. 32 (2007) 944–949;
(b) V.N. Patange, R.K. Pardeshi, B.R. Arbad, Transition metal complexes with oxygen donor ligands: a synthesis, spectral, thermal and antimicrobial study, J. Serb. Chem. Soc. 73 (2008) 1073.
[14] V.D. John, G. Kuttan, K. Krishanankutty, Anti-tumour studies of metal chelates of synthetic curcuminoids, J. Exp. Clin. Can. Res. 21 (2002) 219–224.
[15] H.J.J. Pabon, A synthesis of curcumin and related compounds, Reac. Trav. Chim. 83 (1964) 379–386.
[16] R.C. Srimal, B.N. Dhawan, Anti-thrombotic effect of curcumin, J. Pharma. Pharmacol. 25 (1973) 447–452.
[17] G. Vanangamudi, M. Subramanian, G. Thirunarayanan, Synthesis, spectral linearity, antimicrobial, antioxidant and insect antifeedant activities of some 2,5-dimethyl-3- thienyl chalcones, Arab. J. Chem. (2013).
[18] G. Thiru Narayanan, Synthesis and spectral linearity in substituted styryl 4-Methyl-1-naphthyl ketones, J. Korean Chem. Soc. 52 (4) (2008) 369–379.
[19] G. Thirunarayanan, P.A. Nadar, Am. J. Chem 14 (2002) 1518–1522.
[20] J.N. Dominguez, J.E. Charris, G. Lobo, N. Gamboade Dominguez, M.M. Moreno, F. Riggione, E. Sanchez, J. Olson, P.J. Rosenthal, Synthesis of quinolinyl chalcones and evaluation of their antimalarial activity, Eur. J. Med. Chem. 36 (2001) 555–560.
[21] (a) H.K. Hsieh, L.T. Tsao, C.N. Lin, Synthesis and anti-inflammatory effect of chalcones, J. Pharm. Pharmacol. 52 (2000) 163–171;
(b) F. Herencia, M.L. Ferrandiz, M.J. Alcaraz, Novel anti-inflammatory chalcones derivatives inhibit the induction of nitric oxide synthesis and cyclooxygenase-2 in mouse peritoneal macrophages, FEBS Lett. 453 (1999) 129–134.
[22] M. Chen, L. Zhai, S.B. Christensen, T.G. Theander, A. Kharazmi, Inhibition of fumarate reductase in Leishmania major and L. donovani by chalcones, Agents Chemother. 45 (2001) 2023–2029.
[23] R. DeVincenzo, C. Ferlini, M. Distefano, C. Gaggini, A. Riva, E. Bombardelli, P. Morazzoni, P. Valenti, F. Belluti, F.O. Ranelletti, In vitro evaluation of newly developed chalcones analogues in human cancer cells, Cancer Chemother. Pharmacol. 46 (2000) 305–312.
[24] O.V. Yarishkin, H.W. Ryu, J.Y. Park, M.S. Yang, S.G. Hong, K.H. Park, Sulfonate chalcone as new class voltage-dependent K channel blocker, Bioorg. Med. Chem. 18 (2008) 137–140.
[25] G. Jennings, M.D. Smith, S.M. Kuang, L.M. Hodges, J. Tyrell, R.T. Williamson, P. Seaton, Orthorhombic polymorphs of 1-phenyl-3-(3-hydroxyphenyl)-2-propen-1-one, J. Chem. Cryst. 42 (2012) 159–164.
[26] S. Thabti, A. Djedouani, S. Rahmouni, R. Touzani, A. Bendaas, H. Mousser, A. Mousser, Synthesis, X-ray crystal structures and catecholase activity investigation of new chalcone ligands, J. Mol. Struct. 1102 (2015) 295–301.
[27] A. Altomare, G. Cascarano, C. Giacovazzo, A. Guagliardi, J. Appl. Crystallogr. 26 (1993) 343–350.
[28] G.M. Sheldrick, SHELX97 — Program for Crystal Structure Analysis (Release 97-2), Göttingen, Germany, 1998.
[29] R. Ennington, T. Keith, J. Millam, Shawnee Mission K.S, GaussView, Version. 5, Semichem. Inc., 2009.
[30] A.L. Spek, Structure validation in chemical crystallography, Acta Cryst. D65 (2009) 148–155.
[31] S.K. Wolff, D.J. Grimwood, J.J. McKinnon, D. Jayatilaka, M.A. Spackman, Crystal explorer 2.1, University of Western Australia, Perth, 2007.
[32] B.T. Thaker, R.S. Barvalia, Microwave assisted synthesis and characterization of unsymmetrical tetradentate Schiff base complexes of VO(IV) and MoO(V), Spectrochim. Acta A 84 (2011) 51–61.
[33] M.T. Huang, Z.Y. Wang, C.A. Georgiadis, J.D. Laskin, A.H. Conney, Inhibitory effects of curcumin on tumor initiation by benzo[a]pyrene and 7,12-dimethylbenz[a]anthracene, Carcinogenesis 13 (11) (1992) 2183–2186.
[34] V.N. Patange, B.R. Arbad, Synthesis, spectral, thermal and biological studies of transition metal complexes of 4-hydroxy-3-[3-(4-hydroxyphenyl)- acryloyl]-6-methyl-2H-pyran-2-one, J. Serb. Chem. Soc. 76 (9) (2011) 1237–1246.
[35] B.T. Thaker, R.S. Barvalia, Bidentate coordinating behavior of chalcone based ligands towards oxocations: VO(IV) and Mo(V), Spectrochim. Acta A 112 (2013) 101–109.
[36] R.M. Issa, A.M. Khedr, H.F. Rizk, Antibiotic susceptibility testing by standardized single disc method, Spectrochim. Acta. A 62 (2005) 621–629. Chem. Soc. 76(2011) 1237–1246.
[37] A.W. Bauer, W.M. Kirby, J.C. Sherris, M. Turck, Antibiotic susceptibility testing by standardized single disc method, Am. J. C. Pathol. 44 (1996) 493–496.
[38] A. Altomare, G. Cascarano, C. Giacovazzo, A. Guagliardi, Completion and refinement of crystal structures with *SIR*92, J. Appl. Cryst. 26 (1993) 343–350.
[39] L.P. Nitha, R. Aswathy, N.E. Mathews, B.S. Kumari, K. Mohanan, Synthesis, spectroscopic characterisation, DNA cleavage, superoxidasedismutase activity and antibacterial properties of some transition metal complexes of a novel bidentate Schiff base derived from isatin and 2-aminopyrimidine, Spectrochim. Acta A 118 (2014) 154–161.
[40] N. Raman, Y. Pitchaikaniraja, A. Kulandaisamy, Synthesis and characterisation of Cu(II), Ni(II), Mn(II), Zn(II) and VO(II) Schiff base complexes derived from o-phenylenediamine and acetoacetanilide, Indian Acad. Sci. 113 (2001) 183–189.
[41] A. Bouchama, A. Bendaas, C. Chiter, A. Beghidja, A. Djedouani, Bis(3-acetyl-6-methyl-2-oxo-2H-pyran-4-olato)bis(dimethylformamide) copper(II), Acta Cryst. E63 (2007) m2397.
[42] H. Liang, Q. Yu, R.X. Hu, Z. Yuan Zhou, X-Ge Zhou, Synthesis, crystal structure and spectroscopic properties of a copper(II) complex of the Schiff-base derived from picolinaldehyde N-oxide and 4-aminoantipyridine, Trans. Met. Chem. 27 (2002) 454–457.
[43] W.X. Zhang, C.-Q. Ma, S.-F. Si, Synthesis, structure and electrochemistry of a copper (II) complex with 1,2-di{o-[o-hydroxy(naphthylideneimino)]phenoxy} ethane, Trans. Met. Chem. 26 (2001) 380–383.
[44] H. Xiao, C. Zeng, H. Tian, L. Hu, R. Daniel, Xiao, Electrochemical synthesis of 3,5-disubstituted isoxazoles, J. Electroanal. Chem. 727 (2014) 120–124.
[45] M. Keerati, T.N. Sharanappa, Electrochemical behavior of chalcone at a glassy carbon electrode and its analytical applications, Am. J. Anal. Chem. 3 (2012) 656–663.
[46] N. Deligonul, M. Tumer, Synthesis, characterization, catalytic, electrochemical and thermal properties of tetradentate Schiff base complexes, Trans. Met. Chem. 31 (2006) 920–929.
[47] A. Khander, B. Shaabani, F. Belaj, A. Bakhtiari, Synthesis, characterization and spectroscopic and electrochemical studies of new axially coordinated cobalt (III) salen (salen= N, N′-bis (salicylidene)-1,2-ethylenediamine) complexes. The crystal structure of [Co III (salen)(aniline) 2] ClO_4, Polyhedron 25 (2006) 1893–1900.
[48] M.A. Spackman, D. Jayatilaka, Hirshfeld surface analysis, Cryst. Engg. Comm. 11 (2009) 19–32.
[49] M.A. Spackman, J.J. McKinnon, Fingerprinting intermolecular interactions in molecular crystals, Cryst. Engg. Comm. 4 (2002) 378–392.
[50] I. Warad, A. Barakat, Synthesis, physicochemical analysis of two new hemilabile ether-phosphine ligands and their first stable bis-ether-phosphine/Cobalt(II) tetrahedral complexes, J. Mol. Struct. 1134 (2017) 17–24.
[51] R.S. Mulliken, Electronic population analysis on LCAO-MO molecular wave functions* I, J. Chem. Phys. 23 (1955) 1833–1840.
[52] S. Thirunarayanan, V. Arjunan, M.K. Marchewka, S. Mohan, Y. Atalay, Structure, vibrations and quantum chemical investigations of hydrogen bonded complex of bis(1–hydroxy–2–methylpropan–2–aminium)selenate, J. Mol. Struct. 1107 (2016) 220–230.
[53] N.J. Jasmine, C. Arunagiri, A.S. Stanley, P. Muthiah, Synthesis, X-ray structure analysis, thermodynamic and electronic properties of 4-acetamido benzaldehyde using vibrational spectroscopy and DFT calculations, J. Mol. Struct. 1130 (2017) 244–250.